15th Triennial World Congress, Barcelona, Spain

MOTION CONTROL OF LINEAR SYNCHRONOUS MOTORS WITH FORCE RIPPLE COMPENSATION USING CURRENT SHAPING

Christof Röhrig * **Andreas Jochheim** **

* *Department of Electrical Engineering*
University of Hagen
D-58084 Hagen, Germany

** *Hesse & Knipps GmbH*
Vattmannstraße 6
D-33100 Paderborn, Germany

Abstract: The main problem in improving the tracking performance of linear synchronous motors is the presence of force ripple caused by the irregular magnetic field of the permanent magnets and inaccuracy in electronic commutation by the servo amplifier. In this paper a method to compensate the force ripple based on shaping of the phase current waveforms is presented. The method generates optimized current waveforms which produces minimal copper losses and maximize motor efficiency. The current waveforms are based on a Fourier series approximation. A comparison of the tracking performance with and without force ripple compensation is given. *Copyright © 2002 IFAC*

Keywords: motor control, force ripple, linear motors, optimization.

1. INTRODUCTION

Permanent magnet (PM) linear synchronous motors (LSM) are beginning to find widespread industrial applications, particularly for tasks requiring a high precision in positioning such as various semiconductor fabrication and inspection processes (Basak, 1996). PM LSMs have better performance and higher power density than their induction counterparts (Gieras and Zbigniew, 1999). The main benefits of PM LSMs are the high force density achievable and the high positioning precision and accuracy associated with the mechanical simplicity of such systems. The electromagnetic force is applied directly to the payload without any mechanical transmission such as chains or screw couplings. This greatly reduces nonlinearities and disturbances caused by backlash and additional frictional forces (Pritschow, 1998). Todayt's state-of-the-art linear motors can, typically, achieve velocities up to $10\,m/s$ and accelerations of $10\,g$ (Howe *et al.*, 2001).

The more predominant nonlinear effects underlying a PM LSM system are friction and force ripple arising from imperfections in the underlying components e.g. irregular magnetic field, inaccuracy of commutation. In order to avoid force ripple different methods have been developed. In(Jahns and Soong, 1996) several techniques of torque ripple minimization for rotating motors are reviewed. The arrangement of the permanent magnets can be optimized to reduce cogging forces (Jung *et al.*, 1999),(Cruise and Landy, 1998). In (Van den Braembussche *et al.*, 1996) a force ripple model is developed and identification is carried out with a force sensor and a frictionless air bearing support of the motor carriage. In (Otten *et al.*, 1997) a neuronal-network based feedforward controller is proposed to reduce the effect of force ripple. Position-triggered repetitive control is presented in (Van den

Braembussche *et al.*, 1998). Other approaches are based on disturbance observers (Schrijver and van Dijk, 1999), (Lin *et al.*, 2000), iterative learning control (Lee *et al.*, 2000) or adaptive control (Xu and Yao, 2000). In (Röhrig and Jochheim, 2001) a force ripple compensation method for PM LSM systems with hardware commutated servo amplifiers was presented. A model based method was chosen, because force ripple is a highly reproducible and time-invariant disturbance.

In this paper a compensation and identification method for software commutated servo amplifiers is proposed. The force ripple compensation is directly integrated in the software commutation module of the motion controller. The waveforms of the phase currents are optimized in order to get smooth force and minimal copper losses. The optimal current waveforms are based on Fourier series approximation and are identified by measuring the control signal in a closed position control.

The paper is organized as follows: In Section 2 the experimental setup is described. In Section 3, a physical model of the PM LSM is derived and explained. In Section 4 the optimization procedure of the phase currents is described. In Section 5 the controller design is presented and a comparison of the tracking performance with and without ripple compensation is given. Finally Section 6 concludes the paper.

2. EXPERIMENTAL SETUP

2.1 *Linear Motor*

The motors considered here are PM LSM with epoxy cores. A PM LSM consists of a secondary and a moving primary. There are two basic classifications of PM LSMs: epoxy core (i.e. non-ferrous, slotless) and steel core. Epoxy core motors have coils wound within epoxy support. These motors have a closed magnetic path through the gap since two magnetic plates "sandwich" the coil assembly (Anorad, 1999). Figure 1 shows an unmounted PM LSM with epoxy core. The

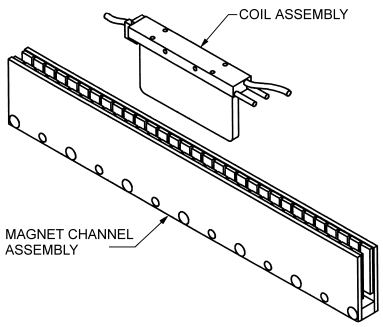

Fig. 1. Anorad LE linear motor

secondary induces a multipole magnetic field in the air gap between the magnetic plates. The magnet assembly consists of rare earth magnets, mounted in alternate polarity on the steel plates. The electromagnetic thrust force is produced by the interaction between the permanent magnetic field in the secondary and the magnetic field in the primary driven by the phase currents of the servo amplifier. The linear motors under evaluation are current-controlled three-phase motors driving carriages supported by roller bearings. Figure 2 shows the Y-axis driven by an Anorad LEA-S-4-S linear motor.

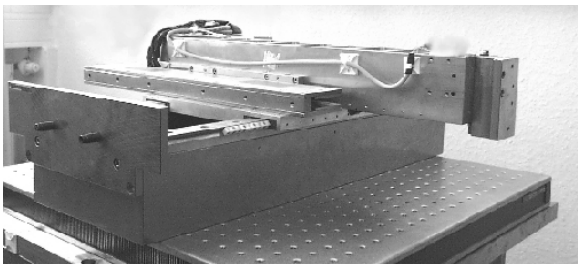

Fig. 2. Experimental setup

2.2 *Servo Amplifier*

The servo amplifiers used in the setup are PWM types with closed current control loop. The software commutation of the three phases is performed in the motion controller with the help of the position encoder. This commutation method requires two current command signals, from the controller, which are $\frac{2\pi}{3}$ apart. The initialization routine for determining the phase relationship is part of the motion controller. The third phase is derived in the servo amplifier:

$$u_3 = -u_1 - u_2$$

Figure 3 shows the block diagram of the Anorad servo amplifier. The maximum input signals u_i of the servo amplifier ($\pm 10V$) correlate to the peak currents of the current loops. In the setup the peak current of the amplifier is $25A$. The PWM works with a switching frequency of $24kHz$. The current loop bandwidth is specified with $2.5kHz$. (Anorad, 1998)

The dynamics of the servo amplifier will not be considered as they play a minor role in the dynamics of the whole system.

3. SYSTEM MODELING

The thrust force is produced by the interaction between the magnetic field in the secondary and the magnetic field of the phase windings. The thrust force is proportional to the magnetic field and the phase currents i_A, i_B, i_C. The back-EMF induced in a phase winding (e_A, e_B, e_C) is proportional to the magnetic

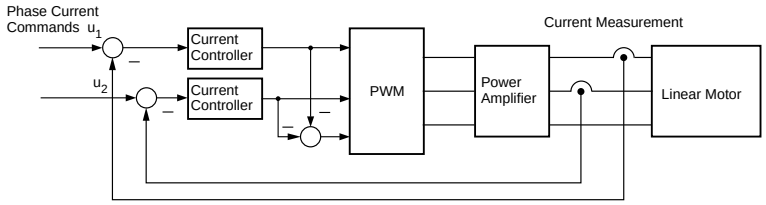

Fig. 3. Block diagram of Anorad servo amplifier

field and the speed of the motor. The total thrust force F_{thrust} is the sum of the forces produced by all phases:

$$\dot{x}F_{thrust} = e_A i_A + e_B i_B + e_C i_C \tag{1}$$

The model of a PM LSM can also be described in the dq-reference frame (Gieras and Zbigniew, 1999). In a PM LSM the reluctance force is negligible and only the current in the q-axis produces force:

$$F_{thrust} = c_\phi \, i_q \tag{2}$$

There are two types of position dependent disturbances: cogging force and force ripple. Cogging is a magnetic disturbance force that is caused by attraction between the PMs and the iron part of the primary. The force depends on the relative position of the primary with respect to the magnets, and it is independent of the motor current. Force ripple is an electro-magnetic effect and causes a periodic variation of the force constant c_ϕ. Force ripple occurs only if the motor current is different from zero, and its absolute value depends on the required thrust force and the relative position of the primary to the secondary. Both disturbances are periodic functions of the position. (Van den Braembussche *et al.*, 1998)

Cogging is negligible in a motor with iron-less primary (Anorad, 1999). Figure 4 shows the nonlinear block diagram of a servo system with PM LSM. The nonlinear disturbances are the velocity depended friction force $F_{friction}$, and the position dependent cogging force $F_{cogging}$ and force ripple $c_\phi(x)$.

The friction force is modeled with a kinetic friction model. In the kinetic friction model the friction force is a function of velocity only. The friction curve is identified with experiments at different velocities. The friction has a discontinuity at $\dot{x} = 0$, because of stiction. A survey of friction models and compensation methods is given in (Amstrong-Hélouvry *et al.*, 1994).

4. CURRENT WAVEFORM OPTIMIZATION

Aim of the current waveform optimization is to obtain a reference waveform of the phase currents which generates smooth force. Only if the back-EMF waveforms are sinusoidal, a sinusoidal current waveform generates ideally smooth force (equation 1). Thus the optimal current waveforms depend directly on the waveforms of the back-EMF.

The main idea of the proposed method is to identify the back-EMF waveforms in a closed position control loop by measuring the control signal u_0 of the position controller at different load forces F_{load} and positions x. Neither additional sensor nor device for position adjustment are necessary. In order to avoid inaccuracy by stiction the measurement is achieved with moving carriage. The position of the carriage is obtained from an incremental linear optical encoder with a measurement resolution of $0.2\mu m$. The experiment consists of several movements at constant low velocity ($1mm/s$) and different load forces ($0 \ldots 70N$). The output of the position controller is stored at equidistant positions. In the identification procedure a sinusoidal reference current is used:

$$\begin{aligned} u_1 &= u_0 \sin\left(\frac{\pi}{\tau_p}(x - x_0)\right) \\ u_2 &= u_0 \sin\left(\frac{\pi}{\tau_p}(x - x_0) - \frac{2\pi}{3}\right) \end{aligned} \tag{3}$$

where u_1, u_2 are the current commands of the two phases, u_0 is the output of the position controller, x is the position of the carriage, τ_p is the pole pitch and x_0 is the zero position with maximum force which is find in an initialization routine.

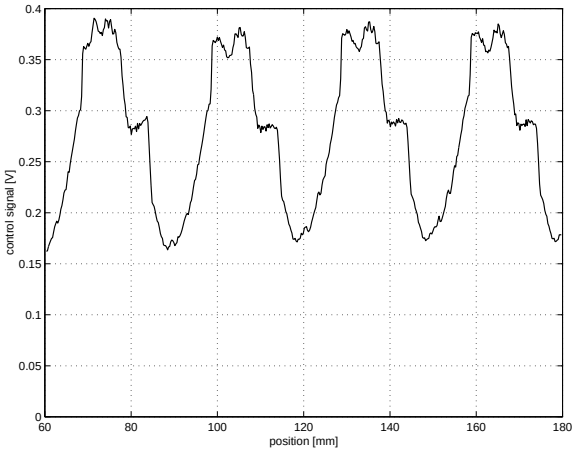

Fig. 5. Control signal at load force F = 20 N

Figure 5 shows the control signal u_0 versus the position x. For analysis of the control signal a least square estimation of the model parameters (function 4) was applied. All harmonics of the controller output are based on the pole pitch τ_p.

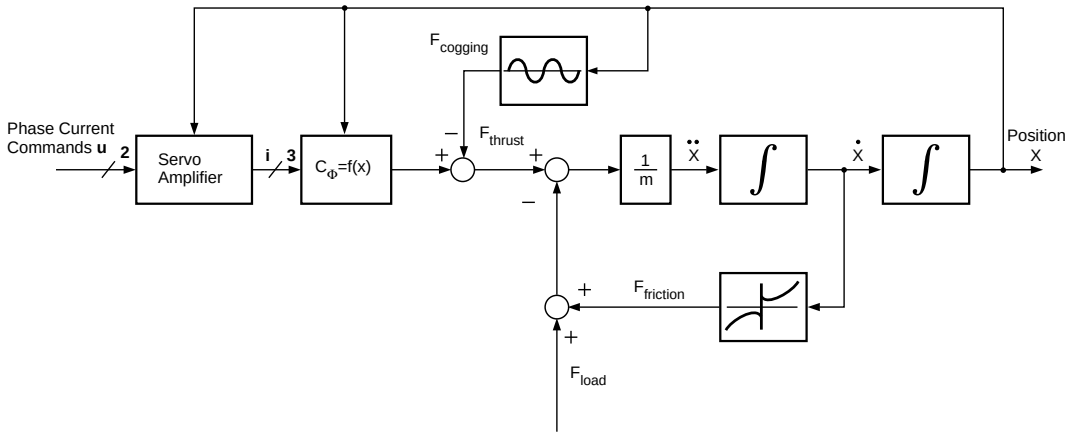

Fig. 4. Nonlinear model of a PM LSM servo system

$$f(x,\theta) = \theta_1 + \sum_{k=1}^{N} \left(\theta_{2k} \sin\left(k\pi\frac{x}{\tau_p}\right) + \theta_{2k+1} \cos\left(k\pi\frac{x}{\tau_p}\right) \right) \quad (4)$$

where θ_k are the estimated parameters.

Figure 6 shows the amplitudes of the sinusoids $\sqrt{\theta_{2k}^2 + \theta_{2k+1}^2}$ versus the corresponding periods $\frac{2\tau_p}{k}$.

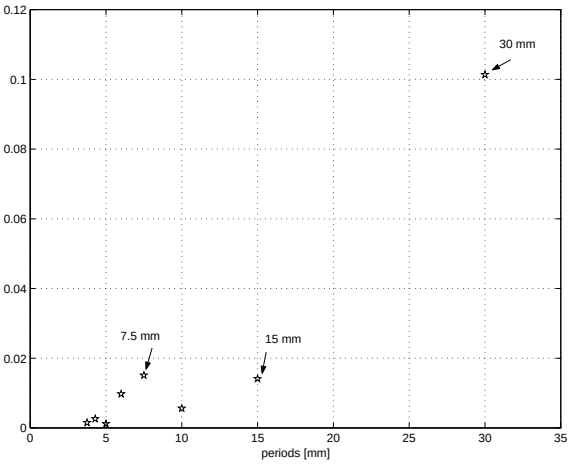

Fig. 6. Spectrum of the force ripple

The fundamental period ($30mm$) correspondents to $2\tau_p$. The amplitude of this sinusoid is independent of the load force. The curves of the phase current commands u_1, u_2 in figure 7 show that the current independent ripple with the period of $2\tau_p = 30.0mm$ are caused by offsets in the analog circuits of the servo amplifier.

In a first step the offsets of the phase current commands are calculated and eliminated in equation 4. In the second step the back-EMF waveforms are identified. Following assumptions are made:

- A constant force is produced with the measured phase currents.

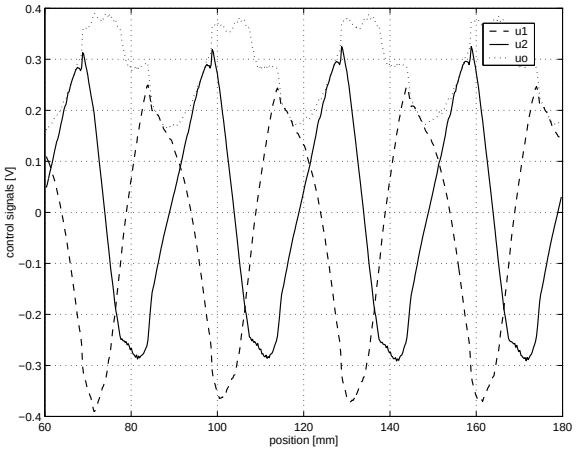

Fig. 7. phase currents at load force F = 20 N

- The product of back-EMF and phase current is proportional to the force contributed by each phase.
- All waveforms are periodic.
- All harmonics of the waveform scale in direct proportion to the fundamental due to the linearity of the motor's basic force equation.

$$\begin{aligned} e_A(x)\,u_1(x) + e_B(x)\,u_2(x) \\ -e_C(x)\,\big(u_1(x) + u_2(x)\big) = \text{ const} \end{aligned} \quad (5)$$

Where $e_A(x)$, $e_B(x)$, $e_C(x)$ are the back-EMFs of the phases A, B, C at a constant velocity, x is the position and u_1, u_2 are the phase current commands. The back-EMFs are calculated in dq-coordinates and then transformed into the phase coordinates A, B, C. After the identification of the back-EMF waveforms, the optimized phase current waveforms are calculated. The optimal current waveforms for generation of smooth force are not uniquely defined unless additional constraints are defined. The constraint considered here are:

- The sum of the phase currents is equal zero.
- Minimum copper losses (i^2R)

The optimization procedure was performed with the MATLAB™ Optimization Toolbox (Mathworks, 1999).

In Figure 8 the calculated and normalized back-EMFs and the optimized phase currents are shown.

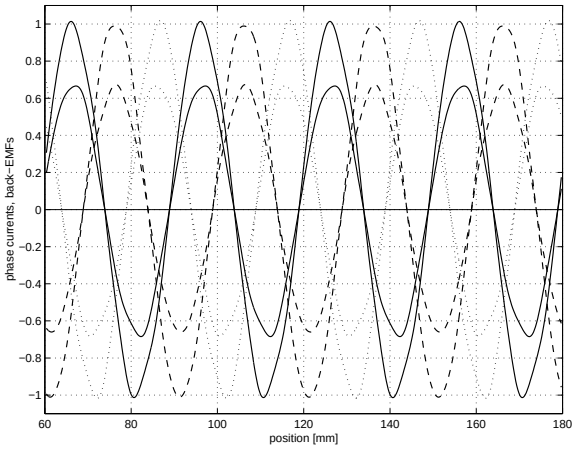

Fig. 8. back-EMFs and phase currents

The result of the optimization procedure are the parameters of function (6) for shaping the phase currents.

$$u_1(x,u_0) = a_1 + \beta_1(x)\,u_0$$
$$u_2(x,u_0) = a_2 + \beta_2(x)\,u_0$$
$$\beta_i(x) = \sum_{k\in M_\beta} b_{ik}\sin\left(\frac{k\pi}{\tau_p}(x+d_{ik})\right) \qquad (6)$$

Where M_β is the set of considered harmonics, x is the position of the carriage, u_0 is the control signal (desired thrust force), u_1, u_2 are the phase currents commands, a_i are the offsets of the servo amplifier inputs, b_{ik} are the amplitudes of the wave shapes, d_{ik} are the phase shifts and τ_p is the pole pitch.

5. CONTROLLER DESIGN

Figure 9 shows the block diagram of the servo control system. In order to achieve a better tracking performance, a feedforward controller is applied. Feedback control without feedforward control always introduces a phase lag in the command response. Feedforward control sends an additional output, besides the feedback output, to drive the servo amplifier input to desired thrust force. The feedforward control compensates the effect of the carriage mass and the friction force. The friction force is modeled by a kinetic friction model and identified with experiments at different velocities. The mass of the carriage is identified with a dynamic least square algorithm. The stability of the system is determined by the feedback loop. The compensation of the force ripple is completely performed in the waveform generator with the help of equations 6. Figure 10 compares the tracking error of a movement without ripple compensation with the movement with ripple compensation. In this measurement, the carriage moves from position 60*mm* to position 180*mm* and back to position 60*mm* with $v_{max} = 200mm/s$. If the ripple compensation is applied, the tracking error is reduced significantly.

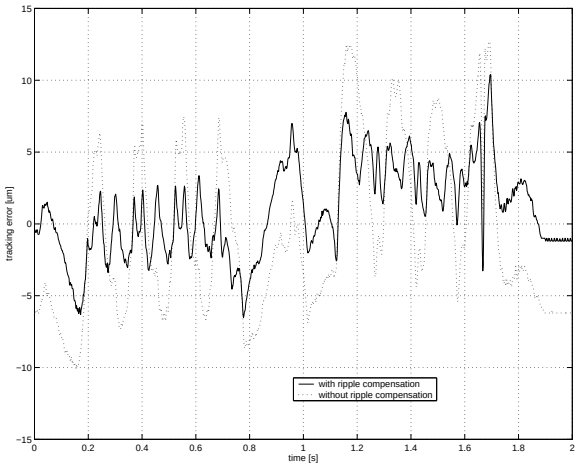

Fig. 10. Tracking error

6. CONCLUSION

In this paper, a motion controller with force ripple compensation is presented. The compensation method based on optimized current waveforms which produces minimal copper losses and maximize motor efficiency. The optimized current shapes are valid for any velocity and thus a static force measurement is possible. In order to identify the model parameters, no additional sensors are required. Experiments show that the tracking performance is significantly improved if the ripple compensation is applied. The described force ripple compensation method is implemented in the motion controller of several machines for semiconductor production to improve the tracking performance.

7. REFERENCES

Amstrong-Hélouvry, B., P. Dupont and C. Canudas de Wit (1994). A Survey of Models, Analysis Tools and Compensation Methods for the Control of Machines with Friction. *Automatica* **30**(7), 1083–1138.

Anorad (1998). *High Voltage Brushless D.C. Servo Amplifier, Hardware Maintenance Manual*. Anorad Corporation.

Anorad (1999). *LE Series Linear Motor Systems, Motor Integration Manual LEA, LEB, LEC & LEM Linear Motors*. Anorad Corporation.

Basak, A. (1996). *Permanent-Magnet DC Linear Motors*. Clarendon Press. Oxford.

Cruise, R.J. and C.F. Landy (1998). Reduction of Detent Forces in Linear Synchronous Motors. In: *Proceedings of the 2th International Symposium on Linear Drives for Industry Applications*. Tokyo, Japan. pp. 412–415.

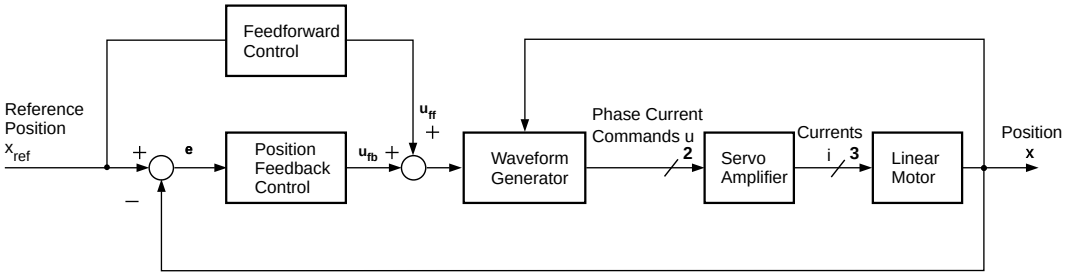

Fig. 9. Force ripple compensation

Gieras, J. F. and J. P. Zbigniew (1999). *Linear Synchronous Motors: Transportation and Automation Systems*. CRC Press. Boca Raton.

Howe, D., R. E. Clark and Z. Q. Zhu (2001). Status of Linear Drive Technologies in Europe. In: *Proceedings of the Third International Symposium on Linear Drives for Industry Applications*. pp. 468–473.

Jahns, T. M. and W. L. Soong (1996). Pulsating Torque Minimization Techniques for Permanent Magnet AC Motor Drives - A Review. *IEEE Transactions on Industrial Electronics* **43**(2), 321–330.

Jung, I.S., J. Hur and D.S. Hyun (1999). 3-D Analysis of Permanent Magnet Linear Synchronous Motor with Magnet Arrangement Using Equivalent Magnetic Circuit Network Method. *IEEE Transactions on Magnetics* **35**(5), 3736–3738.

Lee, T.H., K.K. Tan, S.Y. Lim and H.F. Dou (2000). Iterative Learning of Permanent Magnet Linear Motor with Relay Automatic Tuning. *Mechatronic* **10**(1-2), 169–190.

Lin, F.J., C.H. Lin and C.M. Hong (2000). Robust Control of Linear Synchronous Motor Servodrive Using Disturbance Observer and Recurrent Neural Network Compensator. *IEE Proceedings Electric Power Applications* **147**(4), 263–272.

Mathworks (1999). *Optimization Toolbox User's Guide*. The Mathworks Inc.

Otten, G., T.J.A. de Vries, J. van Amerongen, A.M. Rankers and E.W. Gaal (1997). Linear Motor Motion Control Using a Learning Feedforward Controller. *IEEE/ASME Transactions on Mechatronics* **2**(3), 179–187.

Pritschow, G. (1998). A Comparison of Linear and Conventional Electromechanical Drives. *Annals of the CIRP* **47**(2), 541–548.

Röhrig, C. and A. Jochheim (2001). Identification and Compensation of Force Ripple in Linear Permanent Magnet Motors. In: *Proceedings of the American Control Conference 2001*. pp. 2161–2166.

Schrijver, E. and J. van Dijk (1999). H_∞ Design of Disturbance Compensators for Cogging Forces in a Linear Permanent Magnet Motor. *Journal A* **40**(4), 36–41.

Van den Braembussche, P., J. Swevers and H. Van Brussel (1998). Linear Motor Ripple Compensation Using Position-triggered Repetitive Control. In: *Proceedings of the IFAC Workshop on Motion Control*. Grenoble, France. pp. 353–357.

Van den Braembussche, P., J. Swevers, H. Van Brussel and P. Vanherck (1996). Accurate Tracking Control of Linear Synchronous Motor Machine Tool Axes. *Mechatronics* **6**(5), 507–521.

Xu, L. and B. Yao (2000). Adaptive Robust Precision Motion Control of Linear Motors with Ripple Force Compensations: Theory and Experiments. In: *Proceedings of the IEEE Conference on Control Applications*. pp. 373–378.